Report

Cell Reports

Yap1-Driven Intestinal Repair Is Controlled by Group 3 Innate Lymphoid Cells

Graphical Abstract

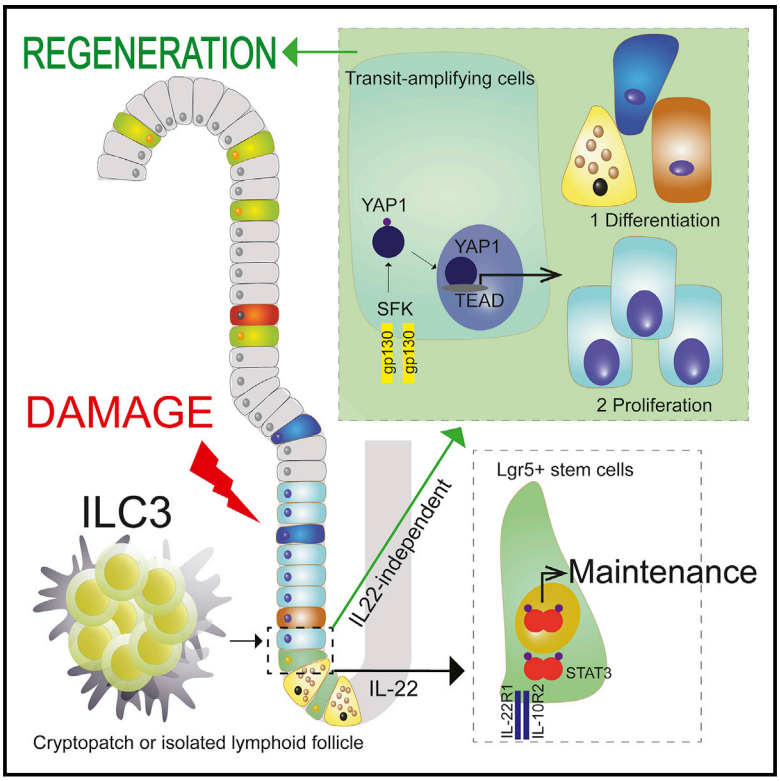

Authors

Mónica Romera-Hernández, Patricia Aparicio-Domingo, Natalie Papazian, ..., Remco M. Hoogenboezem, Janneke N. Samsom, Tom Cupedo

Correspondence

t.cupedo@erasmusmc.nl

In Brief

Intestinal repair is driven by epithelial stem cells, but how these stem cells are instructed to initiate repair was unknown. Here, Romera-Hernández et al. report that epithelial proliferation after damage is independent of the stem cell-protective signal IL-22 but requires ILC3-dependent amplification of regenerative YAP1 signaling in stem cells.

Highlights

- Crypt cell proliferation following small intestinal damage is IL-22 independent
- ILC3s amplify the magnitude of epithelial YAP1 signaling following damage
- Crypt cell proliferation and Lgr5 cell maintenance are independently regulated

Romera-Hernández et al., 2020, Cell Reports *30*, 37–45
January 7, 2020
https://doi.org/10.1016/j.celrep.2019.11.115

CellPress

Cell Reports
Report

Yap1-Driven Intestinal Repair Is Controlled by Group 3 Innate Lymphoid Cells

Mónica Romera-Hernández,[1,3] Patricia Aparicio-Domingo,[1,4] Natalie Papazian,[1] Julien J. Karrich,[1,5] Ferry Cornelissen,[1] Remco M. Hoogenboezem,[1] Janneke N. Samsom,[2] and Tom Cupedo[1,6,*]

[1]Department of Hematology, Erasmus University Medical Center, 3000CA Rotterdam, the Netherlands
[2]Department of Pediatrics, Division of Gastroenterology, Erasmus University Medical Center, 3000CA Rotterdam, the Netherlands
[3]Present address: Terry Fox Laboratory, University of British Columbia, Vancouver, BC, Canada
[4]Present address: Department of Biochemistry, University of Lausanne, Epalinges, Switzerland
[5]Present address: Department of Hematopoiesis, Sanquin Research, Amsterdam, the Netherlands
[6]Lead Contact
*Correspondence: t.cupedo@erasmusmc.nl
https://doi.org/10.1016/j.celrep.2019.11.115

SUMMARY

Tissue repair requires temporal control of progenitor cell proliferation and differentiation to replenish damaged cells. In response to acute insult, group 3 innate lymphoid cells (ILC3s) regulate intestinal stem cell maintenance and subsequent tissue repair. ILC3-derived IL-22 is important for stem cell protection, but the mechanisms of ILC3-driven tissue regeneration remain incompletely defined. Here we report that ILC3-driven epithelial proliferation and tissue regeneration are independent of IL-22. In contrast, ILC3s amplify the magnitude of Hippo-Yap1 signaling in intestinal crypt cells, ensuring adequate initiation of tissue repair and preventing excessive pathology. Mechanistically, ILC3-driven tissue repair is Stat3 independent, but it involves activation of Src family kinases. Our findings reveal that ILC3-driven intestinal repair entails distinct transcriptional networks to control stem cell maintenance and epithelial regeneration, which implies that tissue repair and crypt proliferation can be influenced by targeting innate immune cells independent of the well-established effects of IL-22.

INTRODUCTION

The intestinal epithelium forms a physical barrier that prevents translocation of commensal microorganisms, and defects in intestinal barrier integrity or maintenance have severe clinical impact (König et al., 2016; Peterson and Artis, 2014). Barrier loss activates deleterious immune responses and can lead to transmural ulcers and the need for parenteral nutrition (Sonis, 2004). Such complications are major dose-limiting side effects of high-dose chemotherapy for head-and-neck cancers or during myeloablative conditioning for hematopoietic stem cell transplantation as part of leukemia treatment (Keefe, 2007; Sonis, 2004). Insufficient intestinal barrier repair is a pathological feature underlying inflammatory bowel disease (IBD) (Hollander et al., 1986; Odenwald and Turner, 2013). Continuous bacterial translocation fuels reactivation of microbiota-specific T cells and subsequent disease recurrence in up to 40% of IBD patients in remission (Munkholm et al., 1994). Enhancing intestinal epithelial repair, also coined mucosal healing, has become a sought-after result in experimental and clinical IBD research, yet the cells and signals that enhance epithelial regeneration are still ill defined (Dulai et al., 2015; Florholmen, 2015; Neurath, 2014; Shah et al., 2016).

In contrast to the potentially deleterious consequences of overt antibacterial immune activation following barrier loss, innate immune cell-derived signals positively regulate intestinal regeneration (Aparicio-Domingo et al., 2015; Lindemans et al., 2015). Through production of interleukin (IL)-22, group 3 innate lymphoid cells (ILC3s) safeguard epithelial stem cells after acute small intestinal damage (Aparicio-Domingo et al., 2015). IL-22 is constitutively produced by small intestinal ILC3s (Savage et al., 2017), is important for homeostatic production of antimicrobial peptides (Liang et al., 2006), and drives stem cell proliferation in organoid cultures *ex vivo* (Lindemans et al., 2015).

Intestinal repair is driven by epithelial stem cell differentiation and subsequent proliferation of progenitor cells in crypts of Lieberkühn (Barker, 2014). Crypt regeneration is regulated by signaling pathways activated by signals from local niche cells (Kabiri et al., 2014; Medema and Vermeulen, 2011; Sato et al., 2011). Wnt and Notch signals control stem cell self-renewal (Clevers et al., 2014); in addition, Wnt favors Paneth cell (PC) differentiation (van Es et al., 2005), and Notch controls absorptive versus secretory lineage choices (Tian et al., 2015). Hedgehog signaling drives progenitor proliferation (van Dop et al., 2010), while bone morphogenetic proteins (BMPs) activate the pericryptal mesenchyme to support the epithelial stem cell niche (He et al., 2004). The Hippo-YAP1 pathway is mostly active in response to damage, inhibiting Wnt and Notch signaling to drive early differentiation (Gregorieff et al., 2015; Imajo et al., 2015). IL-22 was also postulated to be a stem cell niche factor, derived not from structural cells but from intestinal ILC3s, and involved in intestinal repair (Hanash et al., 2012; Pickert et al., 2009).

In this study, we set out to define the role of ILC3-derived IL-22 during epithelial repair and to mechanistically interrogate this process. We show that in response to acute small intestinal damage, the stem cell protective cytokine IL-22 is dispensable for crypt cell proliferation and that in contrast, ILC3s modulate

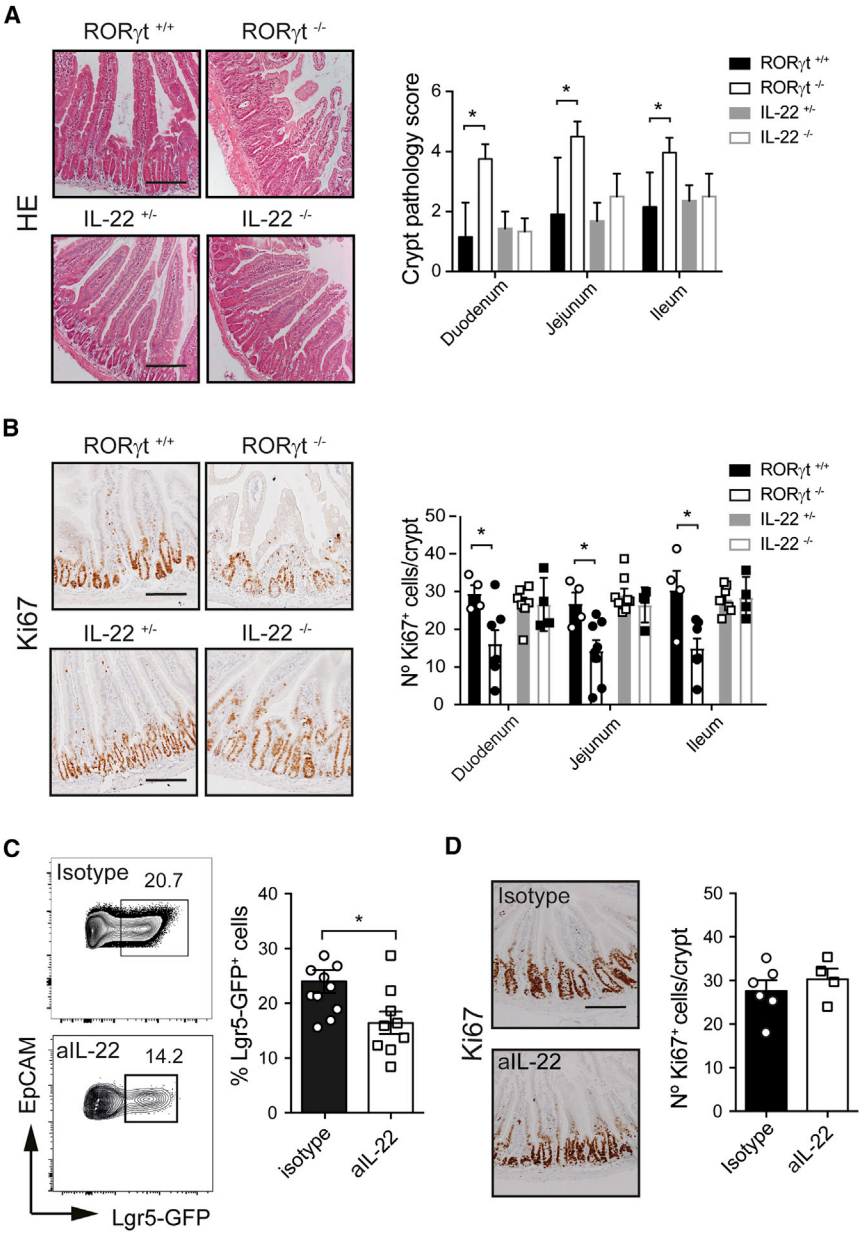

Figure 1. Differential Regulation of Crypt Proliferation and Stem Cell Maintenance

(A) Representative H&E staining and crypt histopathology scores of small intestinal sections from RORγt$^{-/-}$, IL-22$^{-/-}$, and littermate control mice four days after MTX.

(B) Representative Ki67 immunostaining and number of Ki67^{+} cells in small intestinal crypts of RORγt$^{-/-}$, IL-22$^{-/-}$, and littermate control mice four days after MTX.

(C) Representative flow cytometry plots and frequency of Lgr5-GFP^{+} cells in duodenal crypts four days after MTX from Lgr5-GFP$^{+/-}$ mice treated with neutralizing anti-IL-22 antibodies. Numbers indicate the percentage of Lgr5-GFP^{+} cells within Live(+)CD45(−)Ter119(−)CD31(−)EpCAM1(+) cells.

(D) Representative Ki67 immunostaining and number of Ki67^{+} cells in duodenal crypts four days after MTX in Lgr5-GFP$^{+/-}$ mice treated with neutralizing anti-IL-22 antibodies or isotype controls.

Unpaired Mann-Whitney test, *p < 0.01, **p < 0.001; statistically not significant (not indicated). Error bars: SEM. Scale bars: 50 μm; n = 4–8 mice per group. See also Figure S1.

intestinal repair by controlling the amplitude of Hippo-YAP1 signaling. These findings unveil a unique layer of epithelial regulation, in which evolutionary conserved regenerative pathways are amplified by cells of the innate immune system, independent of the well-established effects of IL-22 (Hanash et al., 2012; Lindemans et al., 2015).

RESULTS AND DISCUSSION

Crypt Cell Proliferation after Stem Cell Damage Is IL-22 Independent

The ILC3-derived cytokine IL-22 positively affects recovery of Lgr5^{+} intestinal stem cells from small intestinal crypts after acute damage and induces epithelial proliferation *in vitro* (Aparicio-Domingo et al., 2015; Lindemans et al., 2015). Epithelial repair is independent of adaptive immunity, because proliferation of epithelial cells in response to damage is normal in Rag2$^{-/-}$ mice (Aparicio-Domingo et al., 2015). To determine the importance of IL-22 for small intestinal regeneration, we compared pathology and crypt cell proliferation after methotrexate (MTX)-induced damage in IL-22-deficient mice and ILC3-deficient RORγt$^{-/-}$ mice. As we have shown before, absence of ILC3s increased tissue pathology in response to MTX (Aparicio-Domingo et al., 2015). In contrast, pathology in IL-22-deficient mice was similar to pathology of IL-22-sufficient littermate controls (Figure 1A). As a measure of crypt regeneration, we enumerated proliferating crypt cells during the regenerative phase of the response (day 4). This revealed that the severely reduced proliferation, characteristic of ILC3 deficiency (Aparicio-Domingo et al., 2015), was absent from IL-22$^{-/-}$ animals, in which crypt proliferation was indistinguishable from littermate controls (Figure 1B). We validated the IL-22 deficiency in our colony by generating Th17 cells from spleens and lymph node of naive mice and by isolating total T cells from lamina propria followed by restimulation with IL-23 and transcript analysis of IL-22 (Figure S1A). This led us to hypothesize that small intestinal crypt proliferation after acute MTX-induced damage can occur in an IL-22-independent manner, uncoupled from IL-22-dependent epithelial stem cell maintenance.

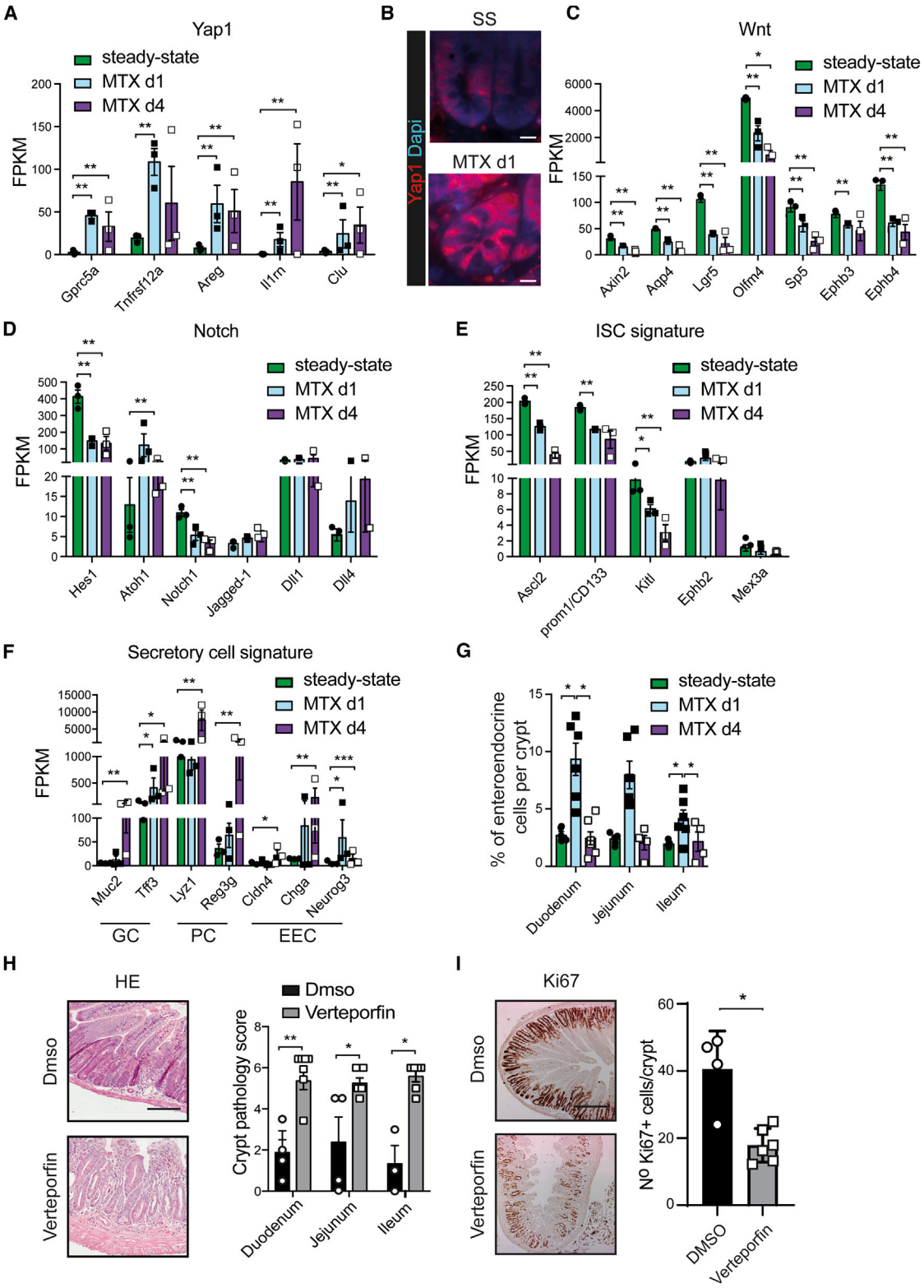

Figure 2. YAP1 Activation Drives Acute Small Intestinal Regeneration

(A) Fragments per kilobase of exon per million fragments mapped (FPKM) values of Yap1 target genes in LGR5-GFP^{hi} crypt cells analyzed by RNA sequencing at steady state (SS), one and four days after MTX.

(legend continued on next page)

To test this hypothesis directly, we neutralized IL-22 by antibody treatment in Lgr5-GFP stem cell-reporter mice during exposure to MTX. This allowed combined analyses of stem cell maintenance and crypt proliferation. Inhibition of IL-22 signaling was confirmed by downregulation of transcripts encoding prototypic IL-22 target genes *Reg3g* and *Reg3b* (Figure S1B). Upon neutralization of IL-22 signaling with antibodies during tissue damage, maintenance of Lgr5-GFP-expressing cells was impaired (Figure 1C). In contrast, crypt proliferation was unaffected (Figure 1D) and was similar to that found in control animals. Altogether, these data reveal that ILC3-dependent stem cell maintenance and crypt proliferation are mechanistically distinct responses to insult and that the early proliferative response following small intestinal injury is IL-22 independent.

YAP1 Signaling Drives Small Intestinal Regeneration

Given that small intestinal crypt proliferation occurred in an IL-22-independent manner, we set out to identify the epithelial repair programs activated by acute small intestinal damage. To this end, we analyzed changes in the epithelial stem cell transcriptome evoked by MTX immediately following induction of damage (day 1) and during regeneration (day 4). RNA sequencing of purified Lgr5-GFP^{hi} crypt cells revealed rapid transcriptional upregulation of target genes of the regeneration-associated Hippo-YAP1 pathway at one and four days after damage (Figure 2A and PCR validation in Figure S2A). Activation of YAP1 involves protein de-phosphorylation and subsequent nuclear translocation. Under homeostatic conditions, YAP1 localization in villus epithelium was exclusively cytoplasmic, while in crypt epithelial cells, both cytoplasmic and faint nuclear localization were observed, suggestive of continuous low-grade YAP1 activation (Figure 2B). MTX exposure induced YAP1 nuclear translocation in crypt epithelial cells (Figure 2B), in line with the increased transcription of YAP1 target genes. Concomitant to YAP1 activation, transcription of genes indicative of WNT (Figures 2C and S2B) and Notch (Figures 2D and S2C) signaling were reduced, in agreement with YAP1-dependent temporal repression of stem cell self-renewal, favoring rapid differentiation at the expense of stemness (Barry et al., 2013; Gregorieff et al., 2015; Yui et al., 2018). Indeed, transcription of genes associated with stem cell identity were reduced (Figure 2E), while transcription of genes associated with mature secretory cells, including goblet cells (GCs), PCs, and enteroendocrine cells (EECs) were all increased (Figures 2F and S2D–S2F), as was the proportion of phenotypic EECs in isolated crypts (Figures 2G and S2G).

YAP1 activates target gene transcription by binding to nuclear TEAD transcription factors (Zhao et al., 2008). The interaction between YAP1 and TEADs can be inhibited by verteporfin, a U.S. Food and Drug Administration-approved drug used for treatment of macular degeneration (Battaglia Parodi et al., 2016). To resolve the importance of YAP1 activation for small intestinal regeneration after MTX-induced damage, we blocked YAP1-TEAD interactions during MTX exposure. YAP1 inhibition increased tissue pathology, characterized by severe crypt abnormalities (Figure 2H) and a significant loss of crypt cell proliferation (Figure 2I), similar to the loss of regeneration in ILC3-deficient RORγt$^{-/-}$ mice. Altogether, these findings identify YAP1 activation as a dominant driver of early small intestinal crypt regeneration following acute damage.

YAP1 Activation Is Blunted in the Absence of ILC3s

Based on the importance of YAP1 activation and ILC3 presence for small intestinal regeneration, we hypothesized that activation of the Hippo-YAP1 pathway is controlled by ILC3 presence. To test this hypothesis, we analyzed YAP1 activation in mice lacking ILC3s. In RORγt-deficient mice, damage-induced YAP1 nuclear translocation was strongly reduced (Figure 3A), leading to a decrease in the percentage of crypts containing at least one cell per transverse section with nuclear YAP1 (Figure 3B) and thus an increase in crypts failing to activate YAP1. To molecularly define crypt responses in the absence of ILC3s, we crossed Lgr5-GFP reporter mice to ILC3-deficient RORγt$^{-/-}$ mice and analyzed the epithelial stem cell transcriptome after small intestinal damage by RNA sequencing. YAP1 activation in LGR5-GFP^{hi} epithelial cells from mice lacking ILC3s was severely blunted, and relative to homeostasis, no significant changes could be detected in most YAP1 target genes (Figures 3C and S3A). Diminished YAP1 activation was concomitant with failure to reduce WNT (Figure 3D) and Notch (Figure 3E) target genes and signaling components and an absence of both loss of stemness (Figure 3F) and induction of transcripts involved in mature secretory cell differentiation (Figure 3G). Similarly, the transient increase in EEC differentiation seen in control crypts (Figure 2G) was absent from crypts from RORγt$^{-/-}$ mice (Figure 3H), highlighting the functional consequences of reduced YAP1 activation. In line with our previous findings on crypt proliferation, transcription of YAP target genes was independent of adaptive immunity and occurred normal in RAG1$^{-/-}$ mice exposed to MTX. In contrast, pretreatment of RAG1$^{-/-}$ mice with Thy1-depleting antibodies to broadly delete innate lymphoid cells (ILCs) hampered induction of YAP targets (Figure S3B). Altogether, these data reveal that the magnitude of Hippo-YAP1 signaling is amplified by presence of small intestinal ILC3s.

(B) Representative YAP1 staining of duodenal sections at the indicated time points after MTX exposure.
(C–F) FPKM values derived from RNA sequencing of LGR5-GFP^{hi} crypt cells of genes involved in (C) Wnt signaling, (D) Notch signaling, (E) intestinal stem cell (ISC) signature, and (F) secretory cell identity, including GCs, PCs, and EECs.
(G) Percentages of EECs in small intestinal crypt-derived cell suspensions analyzed by flow cytometry at the indicated time points. EECs were gated as Live(+) CD45(−)Ter119(−)CD31(−)EpCAM1(+)Lgr5-GFP(−)CD24^{hi}SSC^{lo} cells.
(H) Representative H&E staining and crypt pathology scores of small intestine four days after MTX exposure in the presence of verteporfin or DMSO control.
(I) Representative Ki67 immunostaining and quantification of duodenal sections four days after MTX treatment in the presence of verteporfin or DMSO control.
FPKM values are plotted for transcripts with statistically significant $\log_2$ fold change (DESeq2 analysis of count data) with **adjusted $p < 0.01$, *adjusted $p < 0.05$, or statistically not significant (not indicated). Unpaired Mann-Whitney test, **$p < 0.01$, *$p < 0.05$ (G, H, and I). Error bars: SEM. Scale bars: 10 μm (B), 50 μm (H), 100 μm (I); n = 3 mice per group (A and C–G), n = 4–8 mice per group (B, H, and I). See also Figure S2.

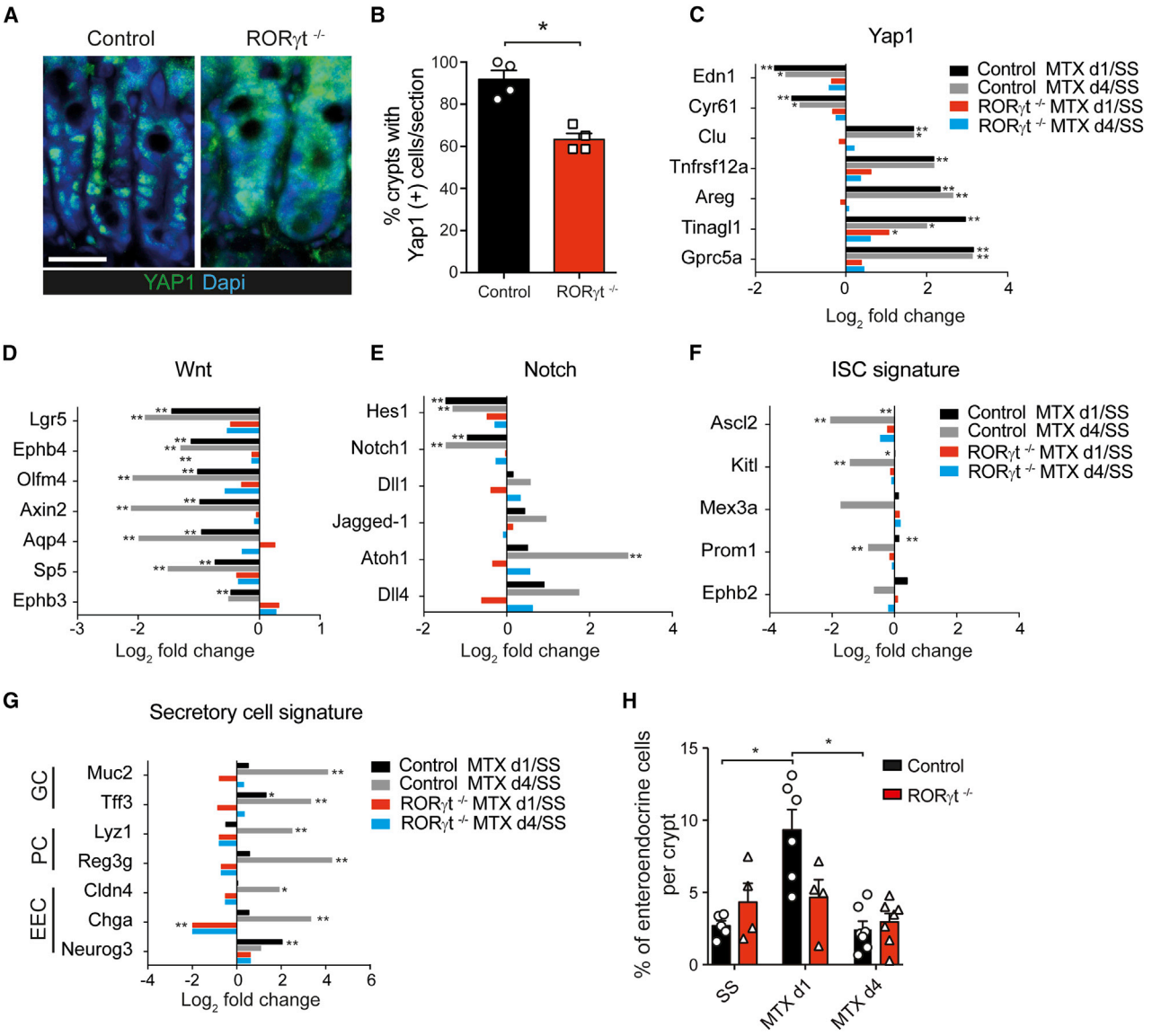

Figure 3. YAP1 Activation Is Blunted in the Absence of ILC3s

(A) Representative YAP1 immunostaining of duodenal crypts from RORγt$^{-/-}$ mice and littermate controls one day after MTX. Scale bar: 50 μm.

(B) Percentage of duodenal crypts containing at least 1 cell with nuclear translocation of YAP1 in RORγt$^{-/-}$ mice and littermate controls one day after MTX.

(C–G) Log_2 fold change values determined by RNA sequencing of Lgr5-GFP^{hi} crypt cells comparing MTX day 1 versus SS for control mice (black bars), RORγt$^{-/-}$ mice (red bars) and MTX day 4 versus SS for control mice (gray bars), or RORγt$^{-/-}$ mice (blue bars) showing (C) YAP1 target genes, (D) Wnt-related genes, (E) Notch-related genes, (F) intestinal stem cell genes, and (G) secretory cell genes.

(H) Percentages of EECs determined by flow cytometry in duodenal crypts at the indicated time points from RORγt$^{-/-}$ mice (red bars). Control mice (as in Figure 2G) are shown for comparison (black bars). EECs were gated as Live(+)CD45(−)Ter119(−)CD31(−)EpCAM1(+)Lgr5-GFP(−)CD24^{hi}SSC^{lo} cells.

Log_2 fold change (DESeq2 analysis of count data) with **adjusted $p < 0.01$, *adjusted $p < 0.05$, or statistically not significant (not indicated) (C–F). FPKM values are plotted for transcripts that have statistically significant log_2 fold change (DESeq2 analysis of count data) with **adjusted $p < 0.01$, *adjusted $p < 0.05$, or statistically not significant (not indicated). Unpaired Mann-Whitney test, *$p < 0.01$; statistically not significant (not indicated) (B and H). Error bars: SEM. n = 4–8 mice per group (A, B, and H), n = 3 mice per group (C–G). See also Figure S3.

Activation of YAP1 Signaling in Intestinal Crypts Is Independent of IL-22

Our findings indicate that crypt proliferation and Lgr5 cell maintenance are independently regulated, fueled by YAP1 and IL-22, respectively. To assess whether IL-22 has a role in epithelial YAP1 activation after small intestinal damage, we quantified YAP1 activation in epithelial stem cells from mice exposed to MTX in the presence of IL-22-neutralizing antibodies. Lgr5-GFP^{hi} crypt cells were analyzed by RNA sequencing one day after MTX. The efficacy of IL-22 neutralization was controlled by analysis of Reg3γ and Reg3β transcription in purified PCs (Figure S3C). IL-22 neutralization did not alter transcripts associated with

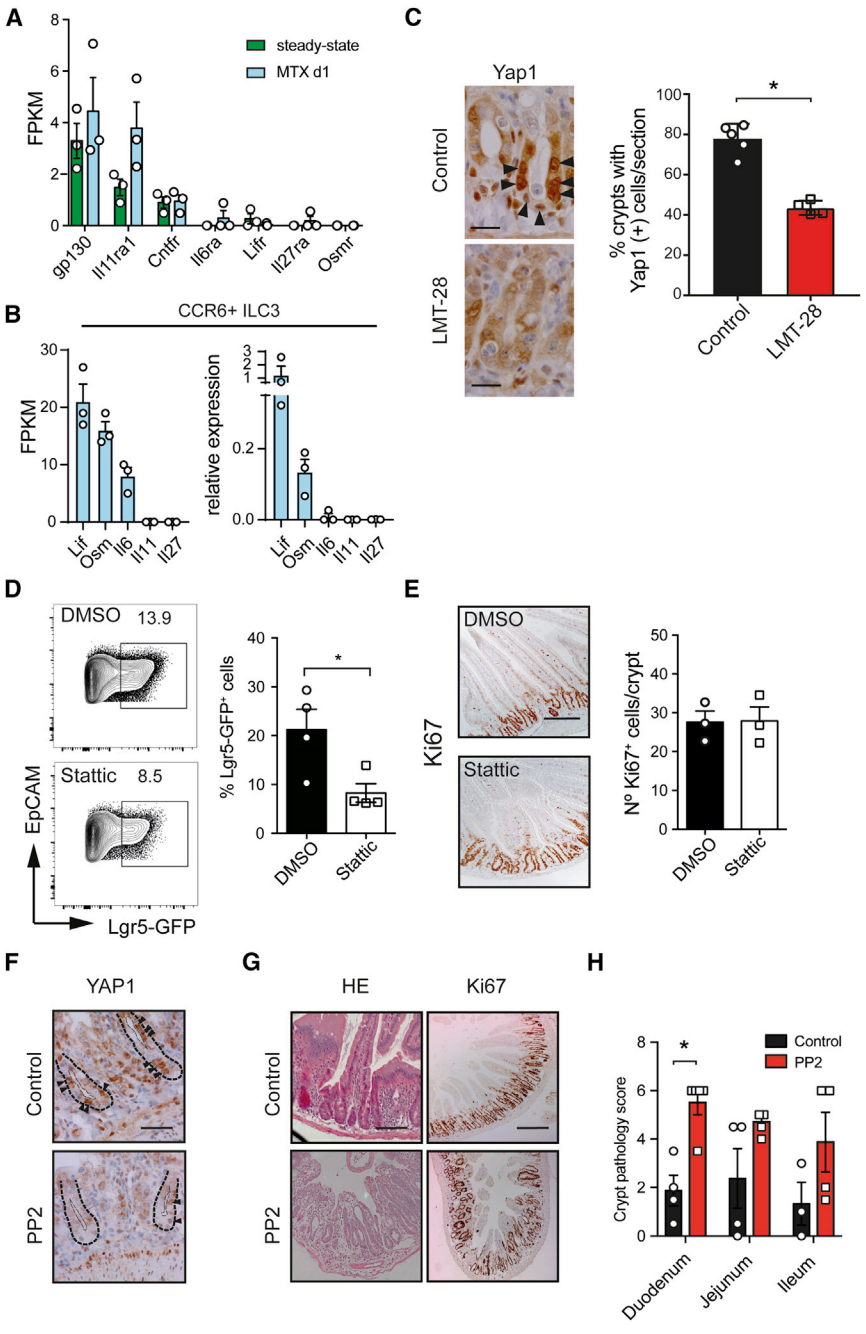

Figure 4. YAP1 Activation Involves gp130-SFK Signaling

(A) FPKM values of gp130 and gp130 co-receptors transcribed by Lgr5-GFP^{hi} crypt cells at steady state and one day after MTX.

(B) FPKM values and relative expression by qPCR of gp130 ligands transcribed by intestinal CCR6^{+}NKp46^{-} ILC3s at steady state.

(C) Representative YAP1 immunostaining and percentage of duodenal crypts containing at least 1 cell with nuclear translocation of YAP1 one day after MTX treatment in the presence of LMT-28 or vehicle control.

(D) Representative flow cytometry plots and frequency of Lgr5-GFP^{+} cells in duodenal crypts four days after MTX from Lgr5-GFP$^{+/-}$ mice treated with STATTIC or DMSO vehicle control. Numbers indicate the percentage of Lgr5-GFP^{+} cells within Live(+)CD45(–)Ter119(–)CD31(–)EpCAM1(+) cells.

(E) Representative Ki67 immunostaining and number of Ki67^{+} cells in duodenal crypts four days after MTX in Lgr5-GFP$^{+/-}$ mice treated with STATTIC or DMSO vehicle control.

(F) Representative YAP1 immunostaining in duodenal crypts from mice treated with SFK inhibitor PP2 or DMSO control one day after MTX.

(G) Representative H&E and Ki67 staining of duodenal sections four days after MTX treatment in the presence of PP2 or DMSO control.

(H) Crypt pathology score of small intestinal sections four days after MTX in mice treated with PP2 or DMSO control.

FPKM values are plotted for transcripts that have statistically significant $\log_2$ fold change (DESeq2 analysis of count data). Unpaired Mann-Whitney test, *$p < 0.01$ (B); unpaired t test, *$p < 0.05$ (C and D). Error bars: SEM. Scale bars: 100 μm (D and F), 50 μm (B); n = 3 mice per group (A, C, and D), n = 4–6 mice per group (B and E–G). See also Figure S4.

YAP1 (Figures S3D and S3E), WNT (Figure S3F), or Notch (Figure S3G) targets or signaling components or transcripts involved in stemness (Figure S3H) or secretory cell differentiation (Figures S3I). These data illustrate that IL-22 signaling is dispensable for YAP1 activation following acute damage to the small intestine.

YAP1 Activation Requires gp130 Dimerization and Src Family Kinase Activation

Damage-induced epithelial YAP1 activation can occur in response to various stimuli, including signaling through the IL-6 family receptor gp130 and mechanotension in response to altered extracellular matrix composition (Taniguchi et al., 2015). Mechanotension-induced YAP1 activation occurs during the later stages of tissue repair and involves activation of a discrete set of genes (Yui et al., 2018). Analyses of these mechanotension-associated genes in Lgr5-GFP^{hi} stem cells after MTX-induced damage showed that these genes are either not transcribed or transcribed at similar levels in ILC3-deficient and control mice (Figures S4A and S4B), making it unlikely that this pathway is important during the initial ILC3-dependent activation of epithelial YAP1.

To define whether ILC3-driven YAP1 involved gp130 signaling, we first analyzed the transcriptome of Lgr5-GFP^{hi} small intestinal crypt cells for the presence of gp130 and the cytokine-specific receptor chains that multimerize with gp130 to form functional receptor units. Under homeostatic conditions, as well as after damage, Lgr5-GFP^{hi} crypt cells transcribed gp130, the il11ra1 chain, and low levels of Cntfr (Figures 4A and S4C). IL-6 can

also signal via a soluble IL-6R that complexes with gp130, thereby precluding the necessity for cell-autonomous IL-6R transcription (Novick et al., 1989). Second, we determined transcription of reciprocal ligands for gp130 receptors by intestinal ILC3s. To this end, we purified CCR6$^+$ ILC3s from the small intestine and performed transcriptional analyses by RNA sequencing and qPCR (Figure 4B). This revealed that small intestinal ILC3s transcribe *Lif*, *Osm*, and likely *Il6*, although there was discrepancy in *Il6* detection by RNA sequencing and PCR (Figure 4B). The IL-6 and IL-11 pathways have been associated with multiple aspects of tissue regeneration, and alterations in these pathways are linked to IBD susceptibility and intestinal cancer progression (Garbers and Scheller, 2013; Katsanos and Papadakis, 2017; Taniguchi and Karin, 2014). Even though ILC3s do not transcribe IL-11, stromal cells can produce IL-11, indicating the possible involvement of a stromal cell relaying ILC3 signals to epithelial cells, a mechanism that we cannot exclude based on our current data. The IL-6 and IL-11 receptors use homo-dimerization of gp130 to form a specific receptor with a single IL-6R or IL-11R chain. To analyze possible involvement of gp130 homo-dimerization in Yap1 activation, we used a small molecule inhibitor of this process (LMT-28) (Hong et al., 2015). LMT-28 application during the induction of small intestinal damage with MTX reduced nuclear translocation of YAP1 in crypt epithelial cells, reduced the percentage of crypts containing at least one cell with nuclear YAP1 per transverse section, and thus increased the number of crypts that failed to activate YAP1-driven regeneration (Figure 4C). Downstream of gp130-associated receptors signals are transduced either by STAT3 signaling or by activation of Src family kinases (SFKs) (Taniguchi et al., 2015). To assess the importance of these two pathways, we inhibited STAT2/3 signaling with the small molecule inhibitor STATTIC and SFK activity with the pharmacological inhibitor PP2. Efficiency of STAT inhibition was controlled by analyses of known STAT3 target genes (Figure S4D). Inhibition of STAT3 signaling also blocks IL-22 receptor signaling, highlighted by the failure of Lgr5$^+$ stem cell maintenance following MTX damage (Figure 4D). In contrast, the YAP1-dependent proliferative response at day 4 after MTX was not affected by STAT2/3 inhibition (Figure 4E), indicating that STAT molecules are not involved in this process. Administration of the SFK inhibitor PP2 prevented nuclear translocation of YAP1 in small intestinal crypt cells (Figure 4F) and resulted in increased crypt pathology and loss of crypt proliferation (Figure 4G), reminiscent of the regenerative defects in ILC3-deficient RORγt$^{-/-}$ mice. These findings again highlight the dichotomy between stem cell maintenance, which is both ILC3 and IL-22 dependent, and crypt proliferation, which is ILC3 dependent yet IL-22 independent.

Collectively, our findings reveal that the evolutionary conserved, regeneration-associated Hippo-YAP1 signaling pathway is amplified by presence of ILC3s, independent of the stem cell-protective effect of IL-22. This implies that immune cell-driven tissue regeneration is the sum of multiple parallel pathways, including the well-established IL-22R signaling pathway, as well as ILC3-dependent YAP1 activation, as shown in this report. The mechanistic uncoupling of stem cell protection and crypt regeneration could suggest that ILC3s act not only on LGR5-expressing intestinal progenitors but also on additional damage-associated epithelial precursor subsets (Ayyaz et al., 2019; Tian et al., 2011).

Our study does not discriminate between direct and indirect epithelial activation by ILC3s. ILC3s may be activating a cell population that functions as an intermediate between ILC3s and epithelial cells, such as crypt-associated mesenchymal stromal cells. Altering the stromal cells adjacent to the intestinal crypts could be part of the mechanistic underpinnings of ILC3-driven tissue repair. Further work is needed to elucidate the exact ILC3- and YAP1-dependent epithelial repair mechanisms.

YAP1-driven intestinal regeneration is critical for epithelial proliferation after intestinal damage in insects (Karpowicz et al., 2010; Ren et al., 2010; Shaw et al., 2010). Nevertheless, ILC3s are present only in mammals and fish (Hernández et al., 2018) and are lacking from more primitive organisms (Lane et al., 2009). Combined with our findings, this implies that evolution favored a complementary layer of crypt regulation driven by specialized innate immune cells. This paves the way for future design of novel targeting strategies aimed at activating ILC3-driven tissue repair in IBD or reducing side effects of anticancer therapies, independent of IL-22.

STAR★METHODS

Detailed methods are provided in the online version of this paper and include the following:

- KEY RESOURCES TABLE
- LEAD CONTACT AND MATERIALS AVAILABILITY
- EXPERIMENTAL MODEL AND SUBJECT DETAILS
- METHOD DETAILS
  - Small intestinal damage
  - Cytokine modulation during MTX treatment
  - Crypt isolation
  - Antibodies
  - Flow cytometry and cell sorting
  - RNA sequencing
  - Histology
  - Immunohistochemistry
  - Transcript analysis
- QUANTIFICATION AND STATISTICAL ANALYSIS
- DATA AND CODE AVAILABILITY

SUPPLEMENTAL INFORMATION

Supplemental Information can be found online at https://doi.org/10.1016/j.celrep.2019.11.115.

ACKNOWLEDGMENTS

Neutralizing IL-22 antibodies and IL-22-deficient mice were provided by Genentech. This work was supported by ZonMW Innovational Research Incentives Vidi grant 91710377 to T.C., Veni grant 91615128 to F.C., and by the People Program (Marie Curie Actions) of the European Union's Seventh Framework Program FP7/2007–2013 under REA grant agreement 289720.

AUTHOR CONTRIBUTIONS

Conceptualization, T.C. and J.N.S.; Investigation, M.R.-H., P.A.-D., N.P., J.J.K., and F.C.; Formal Analysis, M.R.-H., P.A.-D., N.P., J.J.K., F.C., and

R.M.H.; Data Curation, R.M.H.; Writing – Original Draft, M.R.-H. and T.C.; Writing – Review & Editing, T.C. and J.N.S.; Supervision, T.C. and J.N.S.; Funding Acquisition, T.C. and F.C.

DECLARATION OF INTERESTS

The authors declare no competing interests.

Received: June 25, 2019
Revised: October 8, 2019
Accepted: November 27, 2019
Published: January 7, 2020

REFERENCES

Aparicio-Domingo, P., Romera-Hernandez, M., Karrich, J.J., Cornelissen, F., Papazian, N., Lindenbergh-Kortleve, D.J., Butler, J.A., Boon, L., Coles, M.C., Samsom, J.N., and Cupedo, T. (2015). Type 3 innate lymphoid cells maintain intestinal epithelial stem cells after tissue damage. J. Exp. Med. *212*, 1783–1791.

Ayyaz, A., Kumar, S., Sangiorgi, B., Ghoshal, B., Gosio, J., Ouladan, S., Fink, M., Barutcu, S., Trcka, D., Shen, J., et al. (2019). Single-cell transcriptomes of the regenerating intestine reveal a revival stem cell. Nature *569*, 121–125.

Barker, N. (2014). Adult intestinal stem cells: critical drivers of epithelial homeostasis and regeneration. Nat. Rev. Mol. Cell Biol. *15*, 19–33.

Barry, E.R., Morikawa, T., Butler, B.L., Shrestha, K., de la Rosa, R., Yan, K.S., Fuchs, C.S., Magness, S.T., Smits, R., Ogino, S., et al. (2013). Restriction of intestinal stem cell expansion and the regenerative response by YAP. Nature *493*, 106–110.

Battaglia Parodi, M., La Spina, C., Berchicci, L., Petruzzi, G., and Bandello, F. (2016). Photosensitizers and Photodynamic Therapy: Verteporfin. Dev. Ophthalmol. *55*, 330–336.

Clevers, H., Loh, K.M., and Nusse, R. (2014). Stem cell signaling. An integral program for tissue renewal and regeneration: Wnt signaling and stem cell control. Science *346*, 1248012.

de Koning, B.A., van Dieren, J.M., Lindenbergh-Kortleve, D.J., van der Sluis, M., Matsumoto, T., Yamaguchi, K., Einerhand, A.W., Samsom, J.N., Pieters, R., and Nieuwenhuis, E.E. (2006). Contributions of mucosal immune cells to methotrexate-induced mucositis. Int. Immunol. *18*, 941–949.

Dulai, P.S., Levesque, B.G., Feagan, B.G., D'Haens, G., and Sandborn, W.J. (2015). Assessment of mucosal healing in inflammatory bowel disease: review. Gastrointest. Endosc. *82*, 246–255.

Florholmen, J. (2015). Mucosal healing in the era of biologic agents in treatment of inflammatory bowel disease. Scand. J. Gastroenterol. *50*, 43–52.

Garbers, C., and Scheller, J. (2013). Interleukin-6 and interleukin-11: same same but different. Biol. Chem. *394*, 1145–1161.

Gregorieff, A., Liu, Y., Inanlou, M.R., Khomchuk, Y., and Wrana, J.L. (2015). Yap-dependent reprogramming of Lgr5(+) stem cells drives intestinal regeneration and cancer. Nature *526*, 715–718.

Gröschel, S., Sanders, M.A., Hoogenboezem, R., de Wit, E., Bouwman, B.A.M., Erpelinck, C., van der Velden, V.H.J., Havermans, M., Avellino, R., van Lom, K., et al. (2014). A single oncogenic enhancer rearrangement causes concomitant EVI1 and GATA2 deregulation in leukemia. Cell *157*, 369–381.

Hanash, A.M., Dudakov, J.A., Hua, G., O'Connor, M.H., Young, L.F., Singer, N.V., West, M.L., Jenq, R.R., Holland, A.M., Kappel, L.W., et al. (2012). Interleukin-22 protects intestinal stem cells from immune-mediated tissue damage and regulates sensitivity to graft versus host disease. Immunity *37*, 339–350.

He, X.C., Zhang, J., Tong, W.-G., Tawfik, O., Ross, J., Scoville, D.H., Tian, Q., Zeng, X., He, X., Wiedemann, L.M., et al. (2004). BMP signaling inhibits intestinal stem cell self-renewal through suppression of Wnt-beta-catenin signaling. Nat. Genet. *36*, 1117–1121.

Hernández, P.P., Strzelecka, P.M., Athanasiadis, E.I., Hall, D., Robalo, A.F., Collins, C.M., Boudinot, P., Levraud, J.P., and Cvejic, A. (2018). Single-cell transcriptional analysis reveals ILC-like cells in zebrafish. Sci. Immunol. *3*, eaau5265.

Hollander, D., Vadheim, C.M., Brettholz, E., Petersen, G.M., Delahunty, T., and Rotter, J.I. (1986). Increased intestinal permeability in patients with Crohn's disease and their relatives. A possible etiologic factor. Ann. Intern. Med. *105*, 883–885.

Hong, S.S., Choi, J.H., Lee, S.Y., Park, Y.H., Park, K.Y., Lee, J.Y., Kim, J., Gajulapati, V., Goo, J.I., Singh, S., et al. (2015). A Novel Small-Molecule Inhibitor Targeting the IL-6 Receptor β Subunit, Glycoprotein 130. J. Immunol. *195*, 237–245.

Imajo, M., Ebisuya, M., and Nishida, E. (2015). Dual role of YAP and TAZ in renewal of the intestinal epithelium. Nat. Cell Biol. *17*, 7–19.

Kabiri, Z., Greicius, G., Madan, B., Biechele, S., Zhong, Z., Zaribafzadeh, H., Edison, Aliyev, J., Wu, Y., Bunte, R., et al. (2014). Stroma provides an intestinal stem cell niche in the absence of epithelial Wnts. Development *141*, 2206–2215.

Karpowicz, P., Perez, J., and Perrimon, N. (2010). The Hippo tumor suppressor pathway regulates intestinal stem cell regeneration. Development *137*, 4135–4145.

Katsanos, K.H., and Papadakis, K.A. (2017). Inflammatory Bowel Disease: Updates on Molecular Targets for Biologics. Gut Liver *11*, 455–463.

Keefe, D.M. (2007). Intestinal mucositis: mechanisms and management. Curr. Opin. Oncol. *19*, 323–327.

König, J., Wells, J., Cani, P.D., García-Ródenas, C.L., MacDonald, T., Mercenier, A., Whyte, J., Troost, F., and Brummer, R.J. (2016). Human Intestinal Barrier Function in Health and Disease. Clin. Transl. Gastroenterol. *7*, e196.

Lane, P.J., McConnell, F.M., Withers, D., Gaspal, F., Saini, M., and Anderson, G. (2009). Lymphoid tissue inducer cells: bridges between the ancient innate and the modern adaptive immune systems. Mucosal Immunol. *2*, 472–477.

Liang, S.C., Tan, X.-Y., Luxenberg, D.P., Karim, R., Dunussi-Joannopoulos, K., Collins, M., and Fouser, L.A. (2006). Interleukin (IL)-22 and IL-17 are coexpressed by Th17 cells and cooperatively enhance expression of antimicrobial peptides. J. Exp. Med. *203*, 2271–2279.

Lindemans, C.A., Calafiore, M., Mertelsmann, A.M., O'Connor, M.H., Dudakov, J.A., Jenq, R.R., Velardi, E., Young, L.F., Smith, O.M., Lawrence, G., et al. (2015). Interleukin-22 promotes intestinal-stem-cell-mediated epithelial regeneration. Nature *528*, 560–564.

Medema, J.P., and Vermeulen, L. (2011). Microenvironmental regulation of stem cells in intestinal homeostasis and cancer. Nature *474*, 318–326.

Munkholm, P., Langholz, E., Davidsen, M., and Binder, V. (1994). Frequency of glucocorticoid resistance and dependency in Crohn's disease. Gut *35*, 360–362.

Neurath, M.F. (2014). New targets for mucosal healing and therapy in inflammatory bowel diseases. Mucosal Immunol. *7*, 6–19.

Novick, D., Engelmann, H., Wallach, D., and Rubinstein, M. (1989). Soluble cytokine receptors are present in normal human urine. J. Exp. Med. *170*, 1409–1414.

Odenwald, M.A., and Turner, J.R. (2013). Intestinal permeability defects: is it time to treat? Clin. Gastroenterol. Hepatol. *11*, 1075–1083.

Peterson, L.W., and Artis, D. (2014). Intestinal epithelial cells: regulators of barrier function and immune homeostasis. Nat. Rev. Immunol. *14*, 141–153.

Pickert, G., Neufert, C., Leppkes, M., Zheng, Y., Wittkopf, N., Warntjen, M., Lehr, H.A., Hirth, S., Weigmann, B., Wirtz, S., et al. (2009). STAT3 links IL-22 signaling in intestinal epithelial cells to mucosal wound healing. J. Exp. Med. *206*, 1465–1472.

Ren, F., Wang, B., Yue, T., Yun, E.Y., Ip, Y.T., and Jiang, J. (2010). Hippo signaling regulates *Drosophila* intestine stem cell proliferation through multiple pathways. Proc. Natl. Acad. Sci. USA *107*, 21064–21069.

Sato, T., Vries, R.G., Snippert, H.J., van de Wetering, M., Barker, N., Stange, D.E., van Es, J.H., Abo, A., Kujala, P., Peters, P.J., and Clevers, H. (2009). Single Lgr5 stem cells build crypt-villus structures *in vitro* without a mesenchymal niche. Nature *459*, 262–265.

Sato, T., van Es, J.H., Snippert, H.J., Stange, D.E., Vries, R.G., van den Born, M., Barker, N., Shroyer, N.F., van de Wetering, M., and Clevers, H. (2011). Paneth cells constitute the niche for Lgr5 stem cells in intestinal crypts. Nature *469*, 415–418.

Savage, A.K., Liang, H.E., and Locksley, R.M. (2017). The Development of Steady-State Activation Hubs between Adult LTi ILC3s and Primed Macrophages in Small Intestine. J. Immunol. *199*, 1912–1922.

Shah, S.C., Colombel, J.F., Sands, B.E., and Narula, N. (2016). Mucosal Healing Is Associated With Improved Long-term Outcomes of Patients With Ulcerative Colitis: A Systematic Review and Meta-analysis. Clin Gastroenterol. Hepatol. *14*, 1245–1255.

Shaw, R.L., Kohlmaier, A., Polesello, C., Veelken, C., Edgar, B.A., and Tapon, N. (2010). The Hippo pathway regulates intestinal stem cell proliferation during *Drosophila* adult midgut regeneration. Development *137*, 4147–4158.

Sonis, S.T. (2004). The pathobiology of mucositis. Nat. Rev. Cancer *4*, 277–284.

Taniguchi, K., and Karin, M. (2014). IL-6 and related cytokines as the critical lynchpins between inflammation and cancer. Semin. Immunol. *26*, 54–74.

Taniguchi, K., Wu, L.W., Grivennikov, S.I., de Jong, P.R., Lian, I., Yu, F.X., Wang, K., Ho, S.B., Boland, B.S., Chang, J.T., et al. (2015). A gp130-Src-YAP module links inflammation to epithelial regeneration. Nature *519*, 57–62.

Tian, H., Biehs, B., Warming, S., Leong, K.G., Rangell, L., Klein, O.D., and de Sauvage, F.J. (2011). A reserve stem cell population in small intestine renders Lgr5-positive cells dispensable. Nature *478*, 255–259.

Tian, H., Biehs, B., Chiu, C., Siebel, C.W., Wu, Y., Costa, M., de Sauvage, F.J., and Klein, O.D. (2015). Opposing activities of Notch and Wnt signaling regulate intestinal stem cells and gut homeostasis. Cell Rep. *11*, 33–42.

van Dop, W.A., Heijmans, J., Büller, N.V.J.A., Snoek, S.A., Rosekrans, S.L., Wassenberg, E.A., van den Bergh Weerman, M.A., Lanske, B., Clarke, A.R., Winton, D.J., et al. (2010). Loss of Indian Hedgehog activates multiple aspects of a wound healing response in the mouse intestine. Gastroenterology *139*, 1665–1676.

van Es, J.H., Jay, P., Gregorieff, A., van Gijn, M.E., Jonkheer, S., Hatzis, P., Thiele, A., van den Born, M., Begthel, H., Brabletz, T., et al. (2005). Wnt signalling induces maturation of Paneth cells in intestinal crypts. Nat. Cell Biol. *7*, 381–386.

Yui, S., Azzolin, L., Maimets, M., Pedersen, M.T., Fordham, R.P., Hansen, S.L., Larsen, H.L., Guiu, J., Alves, M.R.P., Rundsten, C.F., et al. (2018). YAP/TAZ-Dependent Reprogramming of Colonic Epithelium Links ECM Remodeling to Tissue Regeneration. Cell Stem Cell *22*, 35–49.

Zhao, B., Ye, X., Yu, J., Li, L., Li, W., Li, S., Yu, J., Lin, J.D., Wang, C.Y., Chinnaiyan, A.M., et al. (2008). TEAD mediates YAP-dependent gene induction and growth control. Genes Dev. *22*, 1962–1971.

STAR★METHODS

KEY RESOURCES TABLE

REAGENT or RESOURCE	SOURCE	IDENTIFIER
Antibodies		
Anti IL22 (8E11)	Genentech	N/A
Mouse IgG1 isotype control (MOPC-21)	BioXCell	Cat#BE0083; RRID:AB_1107784
Anti-mouse CD45 (30F11)	Invitrogen	Cat: MCD4517; RRID:AB_10392557
Rat anti-mouse EpCAM1 (G8.8)	Biolegend	Cat# 118218; RRID:AB_2098648
Rat anti-mouse CD24 (M1/69)	Biolegend	Cat# 101814; RRID:AB_439716
Rat anti-mouse CD31 (390)	Biolegend	Cat# 102424; RRID:AB_2650892
Rat anti-mouse Ter119 (TER-119)	Biolegend	Cat# 116234; RRID:AB_2562917
Mouse anti-mouse/rat Ki-67 (MIB-5)	Agilent (Dako)	Cat# M7248; RRID:AB_2142378
Anti-mouse Yap1 (D8H1X)	Cell signaling	Cat# 14074; RRID:AB_2650491
Anti-mouse CD16/CD32 (2.4G2)	BD Biosciences	Cat# 553142; RRID:AB_394657
Chemicals, Peptides, and Recombinant Proteins		
Stattic	Sigma	Cat# S7947
Verteporfin	Selleck Chemicals	Cat # S1786
PP2	Sigma	Cat# P0042
LMT-28	Sigma	Cat# SML1628
XMU-MP-1	Tocris	Cat # 6482
DMSO	Sigma	Cat# 276855-100ML
3,3′-diaminobenzidine tetrahydrochloride	Sigma	Cat# D5905
Tissue-Tek O.C.T compound	Sakura Finetek Europe B.V.	Cat# 4582
Pro-long Gold with DAPI	Invitrogen	Cat# P36935
Clinical grade Methotrexate (Emthexate PF)	Pharmachemie (TEVA group)	Cat# 51.245.305
Critical Commercial Assays		
Vectastain Elite ABC Kit	Vector Laboratories	Cat# PK-6100
NucleoSpin RNA XS kit	Machery Nagel	Cat# 740.902.250
Ovation PicoSL WTA System V2	NuGen	Cat# 3312-48
SensiFAST SYBR Lo-Rox kit	BioLine	Cat# BIO-94050
SMARTer Ultra Low RNA kit	Clontech Laboratories	Cat# 634891
Deposited Data		
Lgr5-GFPhi stem cells; +/− MTX; +/− Rorgt	ArrayExpress	E-MTAB-6639
CCR6+ ILC3 from small intestine	ArrayExpress	E-MTAB-8387
Experimental Models: Organisms/Strains		
Mouse: C57BL/6JOlaHsd	Envigo	https://www.envigo.com/products-services/research-models-services/models/research-models/mice/inbred/c57bl-6-inbred-mice/c57bl-6jolahsd/
Mouse: B6.129P2(Cg)-Rorc^{tm2Litt}/J mice	Jackson	https://www.jax.org/strain/007572
Mouse: IL-22$^{-/-}$	Genentech	N/A
Mouse: Lgr5-GFP-IRES-creERT2	Jackson	https://www.jax.org/strain/008875
Oligonucleotides		
For primer sequences see Table S1		N/A
Software and Algorithms		
CASAVA	Illumina	https://www.illumina.com/
Cutadapt	N/A	https://cutadapt.readthedocs.io/en/stable/
Flowjo v10	Becton Dickinson	https://www.flowjo.com/
Prism 8	GraphPad	https://www.graphpad.com/scientific-software/prism/

LEAD CONTACT AND MATERIALS AVAILABILITY

This study did not generate new unique reagents. Further information and requests for resources and reagents should be directed to and will be fulfilled by the Lead Contact, Tom Cupedo (t.cupedo@erasmusmc.nl).

EXPERIMENTAL MODEL AND SUBJECT DETAILS

C57BL/6, B6.129P2(Cg)-Rorc^{tm2Litt}/J (RORγt-GFP), IL-22$^{-/-}$ (Kindly provided by Genentech, South San Francisco, CA), Lgr5-GFP-IRES-creERT2 (Lgr5-GFP) and Lgr5-GFP/RORγt-GFP mice were bred at the animal facility of the Erasmus University Medical Center Rotterdam. Animal experiments were approved by the institutional review board of the Erasmus University Medical Center in the context of animal experiment license# AVD101002016692. A mix of male and female age-matched mice were used for all experiments.

METHOD DETAILS

Small intestinal damage

8-12 weeks old mice were injected i.p. with 120 mg/kg clinical grade Methotrexate PCH at day-1 and with 60 mg/kg at day 0. Tissues were collected at day 1 and day 4 after the last MTX injection.

Cytokine modulation during MTX treatment

150 μg anti-IL-22 antibody (8E11, kindly provided by Genentech, South San Francisco, CA) or mouse IgG1 isotype control (MOPC-21, BioXCell) were administered i.p to Lgr5-GFP$^{+/-}$ mice every 2 days, starting 4 days before the first MTX dose, until day 2 after the last MTX dose. Stattic (Sigma) was injected at day −1 and day 0 at 0.5 mg/ml in 2.5% DMSO. Control mice were injected with 2.5% DMSO. Verteporfin (Selleckchem) and PP2 (Sigma) were administered at day −1, day 0 and day 1 and mice were analyzed at day 4. Verteporfin was dissolved at a final concentration of 10 mg/injection and PP2 at 1 mg/injection. Both were dissolved in 10% DMSO. Control mice received 10% DMSO. LMT-28 was injected i.p at 5 mg/kg, at days −1, 0 and 2. Control mice were given the same volume of saline containing 10% ethanol.

Crypt isolation

Isolation of intestinal crypts was performed as previously described (Sato et al., 2009). Briefly, isolated small intestines were opened longitudinally and washed with cold PBS. 5 mm pieces were washed with cold PBS, incubated in EDTA (2 mM) at 4°C for 30 min and resuspended in PBS. Crypt-enriched sediments were passed through a 70 μm cell strainer and centrifuged at 200 g for 2 min to separate the crypts from single cells. Crypts were incubated with 1 mL of TrypLE Express (GIBCO) + Dnase I (Merk Millipore) at 37°C for 10-15 min until crypt dissociation was observed. Single cell suspensions were filtered through 40 μm cell strainer and labeled with conjugated antibodies.

Antibodies

The following antibodies were used for flow cytometry: CD45 (30F11; Invitrogen); EpCAM-1 (G8.8), CD24 (M1/69), CD31 (390), Ter119 (TER-119;); all from BioLegend. Dead cells were excluded with 7AAD (Beckman coulter). Antibodies used for paraffin immunostaining were: rat anti-mouse Ki67 monoclonal antibody (MIB-5, Dako) and rabbit anti-mouse Yap1 antibody (D8H1X, Cell signaling).

Flow cytometry and cell sorting

Fc receptors were blocked with appropriate sera or rat-anti-mouse CD16/CD32 (2.4G2; BD Biosciences). All labelings were performed in PBS containing 2% heat-inactivated fetal calf serum (FCS) at 4°C. Labeled cells were analyzed on a FACS LSRII (BD Biosciences) and data processed with FlowJo software (FlowJo, LLC).

RNA sequencing

cDNA was prepared using SMARTer Ultra Low RNA kit (Clontech Laboratories) for Illumina Sequencing following the manufacturer's protocol. For intestinal stem cells and ILC3, sorted cells from 3 individual mice were pooled per data point. The Agilent 2100 Bioanalyzer and the High Sensitivity DNA kit were applied to determine the quantity and quality of the cDNA production. Amplified cDNA was further processed according to TruSeq Sample Preparation v.2 Guide (Illumina) and paired end-sequenced (2x75bp) on the HiSeq 2500 (Illumina). Demultiplexing was performed using CASAVA software (Illumina) and the adaptor sequences were trimmed with Cutadapt (https://cutadapt.readthedocs.io/en/stable/). Alignments against the mouse genome (mm10) and analysis of differential expressed genes were performed with DESeq2 in the R environment on the raw fragment counts extracted from the BAM files by HTSeq-count(Gröschel et al., 2014). Cufflinks software was used to calculate the number of fragments per kilobase of exon per million fragments mapped (FPKM) for each gene.

Histology

Small intestinal tissue pieces (5 mm) or Swiss rolls were fixed in 4% PFA (4h, room temperature), washed in 70% ethanol and embedded in paraffin. Four-μm sections were deparaffinized and stained with hematoxylin (Vector Laboratories) and eosin (Sigma-Aldrich). For Ki67 and YAP1 detection, endogenous peroxidases were blocked in 1% periodic acid in deionized water for 20 min, and antigen retrieval was achieved by microwave treatment in citrate buffer (10mM, pH 6.0). Prior to staining, Fc receptors were blocked in 10% normal mouse serum and 10% of normal serum matching the host species of the secondary antibody, 10 mM Tris buffer, 5 mM EDTA, 0.15 M NaCl, 0.25% gelatin, and 0.05% Tween-20 (pH 8.0). Tissue sections were incubated overnight at 4°C with primary antibodies in PBS supplemented with 2% normal mouse serum. Immunoreactions were detected using biotinylated donkey anti-rat (Dako) and goat-anti-rabbit (Vector Laboratories) and incubated with the Vectastain ABC Elite Kit (Vector Laboratories) and 3,3′-diaminobenzidine tetrahydrochloride (Sigma-Aldrich). Sections were counterstained with hematoxylin. Pathology scores and enumeration of Ki67 and Yap1 were performed blinded. Pathology was scored as previously described (de Koning et al., 2006) and Ki67-expressing cells were counted in 7 to 15 crypts per section.

Immunohistochemistry

Tissues were frozen in Tissue-Tek O.C.T compound (Sakura Finetek Europe B.V.) and stored at −80°C. Six μm cryosections were fixed for 5 min in ice-cold acetone and air-dried for 10 min, and subsequently blocked with 5% normal mouse serum and 5% normal donkey serum for 15 min. Sections were incubated with primary antibody for 1 hr. at room temperature, followed by a 30min incubation with secondary antibodies. Sections were embedded in Pro-long Gold with DAPI (Invitrogen) and analyzed on a Leica DMRXA.

Transcript analysis

RNA was extracted using the NucleoSpin RNA XS kit (Machery Nagel). RNA from sorted cells was amplified with the Ovation PicoSL WTA System V2 (NuGen) according to manufacturer's protocol. For quantitative PCR, a Neviti Thermal Cycler (Applied Biosystems) and SensiFAST SYBR Lo-Rox kit (BioLine) were used, with the addition of $MgCl_2$ to a final concentration of 4 mM. All reactions were performed in duplicate and normalized to the expression of *Gapdh or Cyclophilin*. Relative expression was calculated by the cycling threshold (CT) method as $2^{-\Delta CT}$. The primers sequences can be found in Table S1.

QUANTIFICATION AND STATISTICAL ANALYSIS

Samples were analyzed using unpaired Mann-Whitney test or Unpaired t test as indicated in figure legends. P values < 0.05 were considered significant. Data are shown as mean ± SEM.

DATA AND CODE AVAILABILITY

The accession numbers for the RNA sequencing data reported in this study are ArrayExpress: E-MTAB-6639 and E-MTAB-8387.